Dian J. Borgerink
Robotics and Mechatronics,
CTIT Institute,
University of Twente,
P.O. Box 217,
Enschede 7500 AE, The Netherlands
e-mail: d.j.borgerink@utwente.nl

Dannis M. Brouwer
Associate Professor
Mechanical Automation and Mechatronics,
University of Twente,
P.O. Box 217,
Enschede 7500 AE, The Netherlands
e-mail: d.m.brouwer@utwente.nl

Jan Stegenga
INCAS^3,
P.O. Box 797,
Assen 9400 AT, The Netherlands
e-mail: janstegenga@incas3.eu

Stefano Stramigioli
Professor
IEEE Fellow
Robotics and Mechatronics,
CTIT Institute,
University of Twente,
P.O. Box 217,
Enschede 7500 AE, The Netherlands
e-mail: s.stramigioli@utwente.nl

Kinematic Design Method for Rail-Guided Robotic Arms

For special purpose robotic arms, such as a rail mounted ballast-water tank inspection arm, specific needs require special designs. Currently, there is no method to efficiently design robotic arms that can handle not quantifiable requirements. In this paper, an efficient method for the design and evaluation of the kinematics of manipulator arms on mobile platforms, with certain reach requirements within a limited space, is presented. First, the design space for kinematic arm structures is analyzed and narrowed down by a set of design rules. Second, key test locations in the workspace are determined and reduced based on, for example, relative positions and symmetry. Third, an algorithm is made to solve the inverse kinematics problem in an iterative way, using a virtual elastic wrench on the end effector to control the candidate structure toward its desired pose. The algorithm evaluates the remaining candidate manipulator structures for every required end-effector positions in the reduced set. This method strongly reduces the search space with respect to brute force methods and yields a design that is guaranteed to meet specifications. This method is applied to the use case of a rail-guided robot for ballast-water tank inspection. The resulting manipulator design has been built and the proof of concept has been successfully evaluated in a ballast-water tank replica.
[DOI: 10.1115/1.4035187]

1 Introduction

There is no straightforward method to design the kinematic structure of a manipulator arm. For certain manipulators, generally with a few degrees-of-freedom (DOF), the structure becomes obvious; for example, a gantry or a *xy* table. However, when the task space becomes more complicated, more degrees-of-freedom are required. Since the number of possible structures increases exponentially with the number of joints, heuristic methods or strongly reduced sets are used to generate and evaluate designs. For known static environments, there are some practical guidelines to design manipulators.

However, when the environments become more complicated, these methods cannot guarantee that all required end-effector poses are achievable. Adding redundancy to the manipulator arm by increasing the number of joins might help, but then the question arises of where to add these. Such choices are usually made by a human designer, relying on insights and experience. Inspiration can also be drawn from nature, but this too is a trial-and-error process that relies on a human designer identifying and translating the biological design to a robotic design.

Available robotic arms do not meet the requirements for the purpose in mind. For example, the KUKA lightweight robot [1] and the UR5 from Universal Robotics [2] have separate control boxes and too much mass. The Robolink from Igus [3] is a cable-driven robot arm with a maximum of 5DOF. The pneumatic Bionic Handling Assistant from Festo [4], inspired on an elephant's trunk, is not suitable put on a rail inside ballast water tanks (BWTs) and the dimensions of the JACO^2 from Kinova [5] do not answer the requirements of the use case. For special purpose, manipulator arms such as a ballast water tank custom-tailored designs are required. Additionally, an efficient method to determine the kinematic structure for the robotic arm, so that it is guaranteed to fulfill the requirements, seems nonexistent. Several papers focus on the shape and volume of the workspace, [6,7], limit themselves to three revolute joints, [8,9] or give some general considerations on the design of robot manipulators, [10,11].

Therefore, a novel method to generate and evaluate kinematic structures was created, resulting in a kinematic structure that is guaranteed to reach the required end-effector poses. This paper describes the generic structured method for designing and evaluating the kinematic structure of robotic manipulator arms and applies this method to a specific use case to illustrate its merits.

1.1 Outline. In Sec. 2, the method is presented. First, the kinematic modeling of a manipulator arm is explained. Thereafter, candidate manipulator structures and the workspace will be analyzed, followed by reduction of the number of test locations by utilizing symmetry. Finally, the algorithm used to evaluate the candidate manipulator structures is described. This method is applied to the use case scenario of a ballast water tank inspection robot in Sec. 3. Section 4 presents the simulation results and Sec. 5, a hardware proof of principle of the method applied to this use case. The method is evaluated in Sec. 6 and in Sec. 7, conclusions are drawn.

2 Method

In this section, the proposed method for designing the kinematic structure is presented. The main idea behind this method is to cleverly generate a subset of candidate kinematic structures that are evaluated against a subset of manipulator end-effector poses.

Manuscript received December 16, 2015; final manuscript received November 1, 2016; published online December 22, 2016. Editor: Vijay Kumar.

In contrast with conventional workspace analysis, the orientation of the end effector is taken into account.

The number of candidate structures becomes very large and explodes when the degrees-of-freedom increase. By analyzing possible structures, so-called design rules can be distilled that significantly reduce the set of candidate structures. For example, two adjacent rotational joints with the collinear rotation axes result in a permanent singular Jacobian. The same strategy can be applied to test poses, or end-effector position and orientation. Especially for a rail-guided robot, the set of test poses can be shrunk drastically.

A kinematic model is constructed that can be adapted to the specific candidate structure to be tested. Using this model, an algorithm has been developed to evaluate if the candidate structures can reach the required poses in a systematic way. Since there is generally no closed form solution [12,13], that proves that with a certain structure a pose is reachable or not, the algorithm iteratively tries to reach the final pose within certain limits by means of a virtual spatial spring, an "elastic wrench," between the end effector and the desired pose. The standard Jacobian transpose technique [14], which provides inherent singularity handling capabilities, is implemented to calculate the joint torques from the elastic wrench.

2.1 Kinematic Model. The candidate manipulators are modeled as serial kinematic chains. The homogenous matrix $\mathbf{H}_i^j$ is a general coordinate change from a point in frame Ψ_j to frame Ψ_i

$$\mathbf{H}_i^j = \begin{pmatrix} \mathbf{R}_i^j & \mathbf{p}_i^j \\ \mathbf{0} & 1 \end{pmatrix} \tag{1}$$

with rotation matrix $\mathbf{R}_i^j$, and $\mathbf{p}_i^j$ the coordinates of the origin of Ψ_j expressed in Ψ_i. This homogenous matrix describes the relative configuration of body j with respect to body i. For a serial kinematic chain, these relative configurations can be used to get the configuration of the end effector with respect to the inertial frame Ψ_0 using the chain rule

$$\mathbf{H}_n^0(\mathbf{q}) = \mathbf{H}_1^0(\mathbf{q}_1)\mathbf{H}_2^1(\mathbf{q}_2)\cdots\mathbf{H}_n^{n-1}(\mathbf{q}_n) \tag{2}$$

where q_i denotes the joint variable and $\mathbf{q} := (\mathbf{q}_1 \cdots \mathbf{q}_n)^{\mathrm{T}} \in \Re^{n\times 1}$.

Twists, $\mathbf{T} \in se(3)$, are the generalization of velocities for rigid bodies. Geometrically, they are elements of the Lie algebra $se(3)$ associated to the Lie group $SE(3)$. The twists are a description independent of the configuration, $\mathbf{H}$, and have a pure geometrical interpretation. By applying Mozzi's theorem, any rigid body motion can be expressed as a rotation around an axis and a translation along the same axis. Therefore, any twist can be written as

$$\mathbf{T} = \begin{pmatrix} \boldsymbol{\omega} \\ \mathbf{v} \end{pmatrix} = \underbrace{\begin{pmatrix} \boldsymbol{\omega} \\ \mathbf{r}\wedge\boldsymbol{\omega} \end{pmatrix}}_{\text{rotation}} + \underbrace{\lambda\begin{pmatrix} \mathbf{0} \\ \boldsymbol{\omega} \end{pmatrix}}_{\text{translation}} \tag{3}$$

where

$$\mathbf{r} = \frac{\boldsymbol{\omega}\wedge\mathbf{v}}{\|\boldsymbol{\omega}\|^2} \text{ and } \lambda = \frac{\boldsymbol{\omega}^{\mathrm{T}}\mathbf{v}}{\|\boldsymbol{\omega}\|^2} \tag{4}$$

It can be proven that end-effector twist is the sum of the relative twists, i.e., the contributions of the joints

$$\mathbf{T}_n^{0,0} = \mathbf{T}_1^{0,0} + \mathbf{T}_2^{0,1} + \cdots + \mathbf{T}_n^{0,n-1} \tag{5}$$

In order to describe the kinematics of a rigid robot or a generic rigid mechanism, we need to treat the connection between bodies. This connection is characterized by kinematic pairs or joints. A 1DOF kinematic pair or joint constraints the relative motion of two objects with a unique twist

$$\mathbf{T}_i^{i,i-1} = \hat{\mathbf{T}}_i^{i,i-1}\dot{\mathbf{q}}_i \tag{6}$$

where $\hat{\mathbf{T}}_i^{i,i-1}$ is a constant unit twist. Using Eqs. (5) and (6) and the following notations:

$$\mathbf{T}_i := \hat{\mathbf{T}}_i^{0,i-1} = \mathbf{Ad}_{\mathbf{H}_i^0}\hat{\mathbf{T}}_i^{i,i-1}$$
$$\mathbf{J}(\mathbf{q}) = \begin{pmatrix} \mathbf{T}_1 & \mathbf{T}_2 & \cdots & \mathbf{T}_n \end{pmatrix}$$

the end-effector twist can be described as

$$\mathbf{T}_n^{0,0} = \mathbf{J}(\mathbf{q})\dot{\mathbf{q}} \tag{7}$$

where $\mathbf{J}(\mathbf{q})$ denotes the geometric Jacobian, the columns of the Jacobian are the unit twists expressed in frame Ψ_0. The ith column corresponds to the end-effector twist resulting from a unit angular velocity at joint i while the others are fixed. The dual space of twist is the space of wrenches, $\mathbf{W} \in se^*(3)$, a six-dimensional generalization of forces and velocities. By power continuity, $\mathbf{WT} = \boldsymbol{\tau}\dot{\mathbf{q}}$, it can be seen that the joint torques, $\boldsymbol{\tau}$, can be calculated with

$$\boldsymbol{\tau}^{\mathrm{T}} = \mathbf{J}^{\mathrm{T}}(\mathbf{q})(\mathbf{W}^{0,n})^{\mathrm{T}} \tag{8}$$

More information about geometric modeling of robots can be found in Refs. [13], [15], and [16].

2.2 Scenario Simplification. Usually, the workspace of a robotic arm is expressed with respect to a fixed base. For a rail-mounted system, the reachable workspace is more complicated as the base is able to move along a rail track. It is useful to simplify this scenario. A scenario consists of a set of desired end-effector poses and a rail system on which the base of the robot can position itself. Certain aspects of the scenario can be exploited to obtain a model that is simple yet sufficient. For example, the rail can be

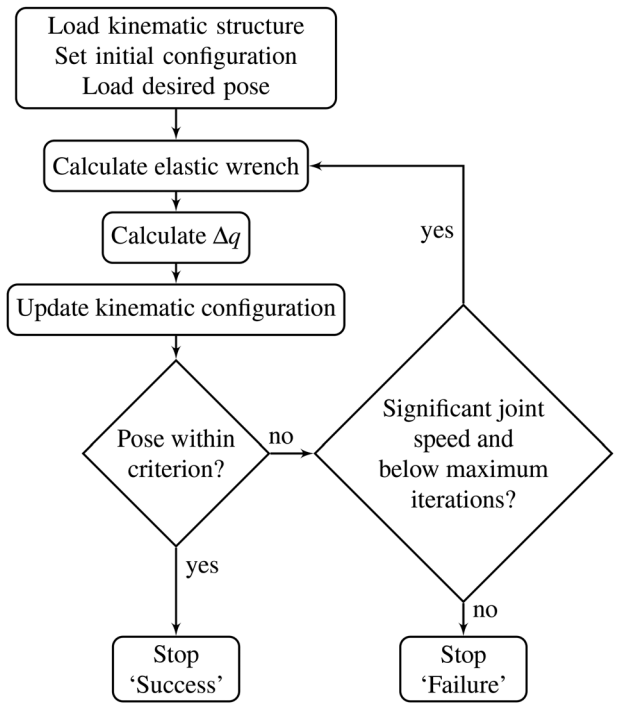

Fig. 1 Evaluation algorithm for test locations given the manipulator structure

installed such that it is parallel to large sections of the walls. It is then possible to define a limited set of target poses for the end effector, which need to be evaluated for reachability.

It is essential to realize that only the relative position and orientation from the base of the manipulator to the required end-effector pose are relevant. Therefore, by identifying the required end-effector positions and choosing base positions, a finite set of relative poses is obtained that should be reachable.

2.3 Algorithm. The algorithm tries to find the inverse kinematics solution for a given manipulator and test location. In general, there is no closed-form solution; there could be one infinite or no solutions at all. Therefore, an algorithm is developed to iterate toward the desired pose, if possible. In Fig. 1, the flowchart that clarifies how the algorithm tries to solve the inverse kinematic problem for a particular test location and manipulator is presented. The algorithm repeats this for every test location for every manipulator structure provided and generates a report on the performance of the structures.

First, the algorithm loads the first manipulator structure, initial configuration, and the first test location. Then the end-effector pose is calculated, using forward kinematics, and its relative configuration with respect to the desired pose, $\mathbf{H}_d^e$, is calculated using

$$\mathbf{H}_d^e = \mathbf{H}_0^e \mathbf{H}_d^0 = \left(\mathbf{H}_e^0\right)^{-1} \mathbf{H}_d^0 = \begin{pmatrix} \mathbf{R}_d^e & \mathbf{p}_d^e \\ \mathbf{0} & 1 \end{pmatrix} \tag{9}$$

$$\left(\mathbf{H}_e^0\right)^{-1} = \begin{pmatrix} \left(\mathbf{R}_e^0\right)^{\mathrm{T}} & -\left(\mathbf{R}_e^0\right)\mathbf{p}_e^0 \\ \mathbf{0} & 1 \end{pmatrix} \tag{10}$$

with the relative rotation matrix $\mathbf{R}_d^e$ and the distance, expressed in end-effector coordinates, $\mathbf{p}_d^e$. When the end-effector pose is at its desired pose, $\mathbf{H}_d^e = \mathbf{I}_4$ holds.

To move the end effector toward the desired pose, a virtual spatial spring is connected between them. A difference between the end effector and the desired poses is translated by this spring to an elastic wrench acting on the end effector.

Based on previous work of Fasse and Broenink [17], Stramigioli [15] presented a completely coordinate-free formulation of a geometric spring connection between two rigid bodies. Instead of connecting a spatial compliance between two rigid bodies, in the proposed algorithm, it is connected between the end effector and the desired end pose. In other words, the rigid body of the desired location could be considered to be connected to the fixed world. The wrench acting on the end effector, expressed in end-effector coordinates, resulting from the relative configuration and the geometric spring can be calculated using

$$\mathbf{W}^e\left(\mathbf{H}_d^e\right) = \begin{pmatrix} \left(\mathbf{m}^e\right)^{\mathrm{T}} & \left(\mathbf{f}^e\right)^{\mathrm{T}} \end{pmatrix} \tag{11}$$

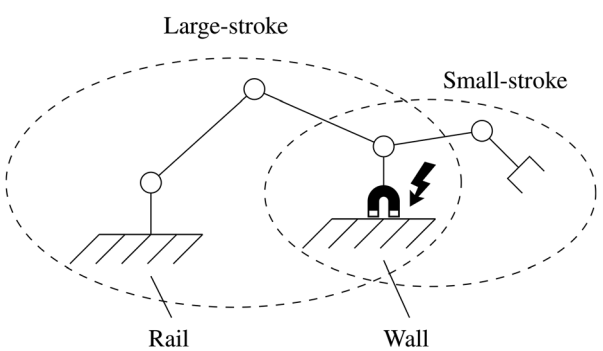

Fig. 2 Two-stage arm concept, with a magnet as intermediate end effector, latching to a wall. Only the large-stroke arm is considered in this study.

$$\tilde{\mathbf{m}}^e = -2\mathbf{as}\left(\mathbf{G}_o\mathbf{R}_e^d\right) - \mathbf{as}\left(\mathbf{G}_t\mathbf{R}_d^e\tilde{\mathbf{p}}_e^d\mathbf{R}_e^d\right) - 2\mathbf{as}\left(\mathbf{G}_c\tilde{\mathbf{p}}_e^j\mathbf{R}_e^d\right) \tag{12}$$

$$\tilde{\mathbf{f}}^e = -\mathbf{R}_d^e\mathbf{as}\left(\mathbf{G}_t\tilde{\mathbf{p}}_e^d\right)\mathbf{R}_e^d - \mathbf{as}\left(\mathbf{G}_t\mathbf{R}_d^e\tilde{\mathbf{p}}_e^d\mathbf{R}_e^d\right) - 2\mathbf{as}\left(\mathbf{G}_c\mathbf{R}_e^d\right) \tag{13}$$

where $\mathrm{as}(\mathbf{A})$ denotes the antisymmetric part of a square matrix A, $\mathrm{as}(\mathbf{A}) := \left(\frac{1}{2}\right)(\mathbf{A} - \mathbf{A}^{\mathrm{T}})$ and the so-called co-stiffness, Fasse and Broenink [17], $\mathbf{G}_x = (1/2)\mathrm{trace}(\mathbf{K}_x)\mathbf{I} - \mathbf{K}_x$, with $x = o, t, c$ for the orientation, translational, and the coupling terms. Furthermore, the tilde operator defines the following one-to-one relation between a point and a mapping of points:

$$\mathbf{x} = \begin{pmatrix} \mathbf{x}_1 \\ \mathbf{x}_2 \\ \mathbf{x}_3 \end{pmatrix} \Longleftrightarrow \tilde{\mathbf{x}} = \begin{pmatrix} 0 & -x_3 & x_2 \\ x_3 & 0 & -x_1 \\ -x_2 & x_1 & 0 \end{pmatrix} \tag{14}$$

The joint torques required to mimic this virtual stiffness are calculated using the standard Jacobian transpose technique, Eq. (8)

$$\boldsymbol{\tau}^{\mathrm{T}} = \mathbf{J}^{\mathrm{T}}\mathbf{Ad}_{\mathbf{H}_0^e}^{\mathrm{T}}\left(\mathbf{W}^e\right)^{\mathrm{T}} \tag{15}$$

with the manipulators Jacobian, $\mathbf{J}$, and the adjoint transformation, $\mathbf{Ad}_{\mathbf{H}_0^e}$, expressing the end-effector wrench, $\mathbf{W}^e$, in the inertial frame. This joint torque is set proportional, κ, to the increase in joint angle used to update the kinematic structure

$$\mathbf{q}_{\mathrm{new}} = \mathbf{q} + \Delta\mathbf{q} = \mathbf{q} + \boldsymbol{\kappa}\boldsymbol{\tau}^{\mathrm{T}} \tag{16}$$

These new joint angles determine the new configuration of the manipulator and are used to calculate the relative configuration again. Before the next iteration step starts, the algorithm performs some evaluations on this step. If the end-effector pose is within the predefined margin of the desired pose, the algorithm labels this test location "success" and moves on to the next test location. On the other hand, if the maximum number of iterations is exceeded or the method is making insufficient progress, $\max(\Delta\mathbf{q})$ is below the threshold, the algorithm labels this test location "failure" and moves on to the next test location. Otherwise, the next iteration step is performed.

When all test locations are evaluated, the algorithm proceeds with the next candidate manipulator structure until all manipulators are evaluated.

For evaluation purposes, additional data are stored for all manipulators and their test locations. For example, the joint angles to visualize the manipulator and the Jacobian are useful to determine the manipulability measure.

3 Implementation

The method described in Sec. 2 is applied to a use case of the design of a manipulator arm for a ballast water tank inspection robot.

3.1 Use Case Scenario: Ballast Water Tank Inspection. Large ships are equipped with ballast water tanks (BWTs), which can be filled in order to increase their stability and to balance ships while, for example, cargo is being unloaded. For obvious reasons, frequent inspection, cleaning, and repairing of coating are required [18]. Up to now, ship owners are obliged to send their ships to dry docks for maintenance, causing the ship to be out of service temporary, which incurs significant costs for owners.

Due to the complex structure of the tanks and additional obstacles such as pipes, stairs, and manholes, it is difficult to automate the maintenance of BWTs. In previous studies, Christensen et al. [19,20] showed that a rail-guided robotic system has the greatest potential.

For the inspection of BWTs, some contact measurements, such as the dry-film thickness, are required [18,21]. Therefore, the robot should be equipped with a robotic manipulator arm, which can take the required measurements at the interior walls. Borgerink et al. [22] indicated that a single manipulator arm practically will not meet the requirements due to the compliance of the proposed rail. A dual stage configuration solves the precision issue of the main arm, see Fig. 2. The large-stroke arm fixes the base of a second arm to the interior wall. The positioning accuracy is ensured by this second arm, relaxing the demands for the large-stroke manipulator arm whose kinematic design is the use case for the presented design method.

3.1.1 Requirements. The requirements for the large-stroke manipulator arm have both a quantifiable and a descriptive nature. For example, the manipulator should be lightweight, reach all "test locations" on the interior walls, and be able to fold to a minimal volume, since it should pass the manholes. The dual-stage concept relaxes the positioning accuracy requirement for the large-stroke arm. Important is that the base of the second manipulator, a permanent electromagnet, is placed perpendicular to the wall; a misalignment up to 5 deg is considered acceptable. The first joint of the second stage is collinear with the magnet. Therefore, the angle of the end effector about the perpendicular axis is indifferent. The reach of the short-stroke arm is $\geq$10 cm and a magnet positioning accuracy of 5 mm is considered sufficient.

Since the orientation of the magnet around its longitudinal axis is indifferent, a minimal of 5DOFs are required. In order to avoid obstacles, like pipes and the rail itself, some redundancy is required. Therefore, a 6DOF manipulator will be designed and evaluated.

3.1.2 Scenario Simplification. The scenario is given by an experimental tank, whose dimensions are known from computer-aided design (CAD). A modular rail system is installed inside the tank. The process of mapping coordinates of the experimental tank to relative locations is explained on the basis of an example. Figure 3 shows a section view of the experimental tank with two arbitrary starting positions on the rail in different compartments. The end effector must be able to reach test locations 1–6 while at root location A, and tank locations 7–9 while at B. When all tank locations are expressed in the frame of their respective root location, see Fig. 3(*a*), the required relative poses are obtained. Note that the orientation of root location B differs from A. The coordinates of the corners are obtained from the CAD drawings of the tank. The required pose of the intermediate end effector is obtained using the coordinates of the corner, the direction of the surface normal, and an offset distance of the corner. The short-stroke arm is considered to have a workspace with a radius of 100 mm; this distance will be used as the offset. The manipulator base pose is obtained from the CAD model; the position on the rail is such that the distance to the test location is minimized and orientation is defined by the location on the rail. From the experimental tank, a set of 303 relative poses is obtained. Many of the poses are similar due to the repetitive geometry of the BWT. When two poses are within an empirically established margin of 4 mm and 1 deg from each other, they are considered one and the other is removed from the set. The remaining set of 169 relative poses will be used as the minimal performance criterion for the kinematic structure. Figure 4 indicates the reduced set of test locations for the test tank.

3.1.3 Manipulator Candidate Structures. The kinematic structure of a manipulator is basically a chain of alternating link and joint elements. The shortest distance between two points is a straight line. Therefore, the structure of the manipulator is chosen such that the manipulator approaches a straight line when it is stretched, minimizing the required material and thereby its weight. Due to the actuators in mind and the mechanical connections, it has been decided to restrict the joints to axial axis, "A-joints," joints perpendicular to the axial axis, "P-joints," and "X-joints," orthogonal to both the axial axis and the previous P-joint.

A brute force method to generate models is to create a model for every possible combination of joint types. In general, for an nDOF system with three types of joints, this would yield 3^n possibilities. For the assumed 6DOF system, this yields 729 possible combinations. Most structures are irrelevant; by exploiting the requirements and the properties of the rail-guided robot, the following design rules will eliminate most models:

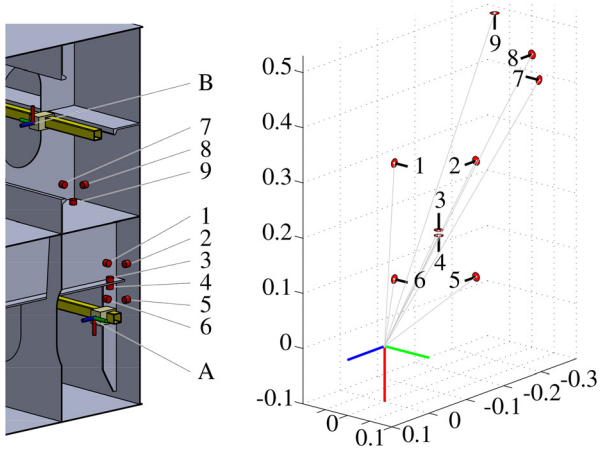

Fig. 3 Mapping of tank locations to relative locations. The relative locations from the tank (left) determine the required workspace (right). The surface normal of the required pose is indicated with a line segment normal to a circle.

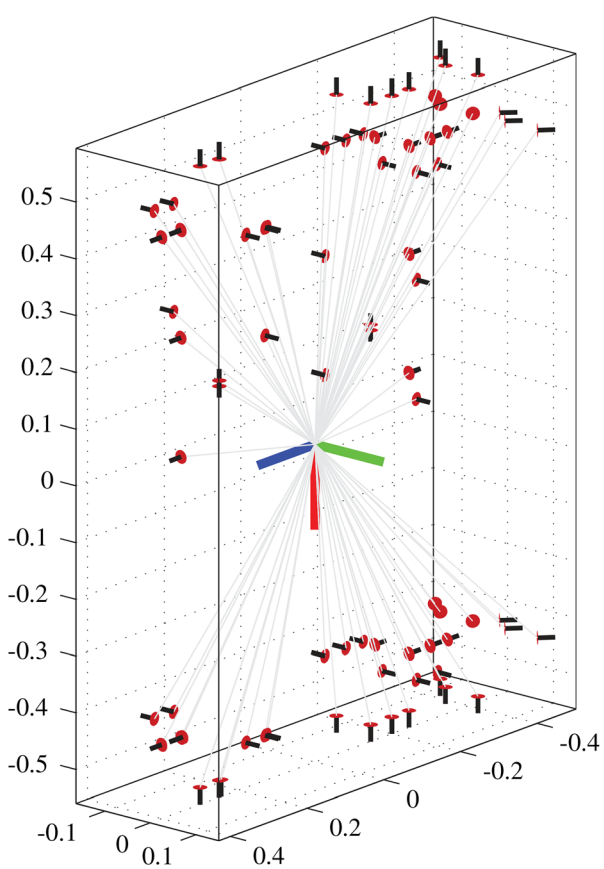

Fig. 4 Reduced set of 169 test locations of the experimental ballast water tank

(1) The longitudinal orientation of the end effector is irrelevant. Therefore, the last joint should not be an A-joint.
(2) For the first joint, an X- or P-joint is unfavorable. Their range is limited to prevent collision with the base.
(3) Two subsequent joints with collinear axes introduce a permanent singular Jacobian.
(4) After an A-joint, X- and P-joints are effectively equal.
(5) To allow maximum rotational dexterity at the end effector, while maintaining maximum reachability, the before last joint must be an A-joint.

The last rule is a consequence of the first; if the last joint could be an A-joint, it would make no sense to implement an A-joint before last joint.

After applying these "elimination rules," only five models remain; these are shown in Fig. 5. A complete kinematic model also requires link lengths, for which the following design rules were used. From the required workspace, a maximum distance of 0.744 m is obtained between base and desired pose. This yields the minimal manipulator length. Foldability is required to shape the robotic arm into a small envelope. This is necessary for maneuvering through manholes and making bends with a radius of 400 mm. The maximum height to pass through manholes is 180 mm; this means, for the candidate structures, that the distance from the base to the first non-A joint must be small. The same reasoning holds for the last link length. In this research, no optimization is done with respect to the link length; they are chosen manually. The longitudinal position of an A-joint essentially does not change the kinematic structure, as long as it fits between the preceding and consecutive joint. Therefore, an A-joint effectively merges two individual link lengths into one effective length. Therefore, the number of relevant link length parameters to be chosen is equal to the number of non-A joints plus one. For example, structure M005 in Fig. 5 has four effective link lengths. To leave space to attach the second stage arm, a link length, including the electromagnet, of 100 mm was chosen. Furthermore, for a compact envelope, the first link length should be minimal. After a design study, the first effective link length turned out to be of a minimal length of approximately 50 mm, and the dimension is limited by the available sizes of the bearing and motors.

3.1.4 Simulation. The five remaining kinematic structures are evaluated with the algorithm described in Sec. 2.3 for all 169 test locations. Based on the use case requirements, the pose-error margin is set to a position error of $d_{cr} = 5$ mm and the end effector must be perpendicular to the interior wall, with a maximum deviation of $\alpha_{cr} = 5$ deg. The maximum number of iterations per test location is empirically set to 10^4, which is significantly above the average iterations required to reach the desired end-effector pose.

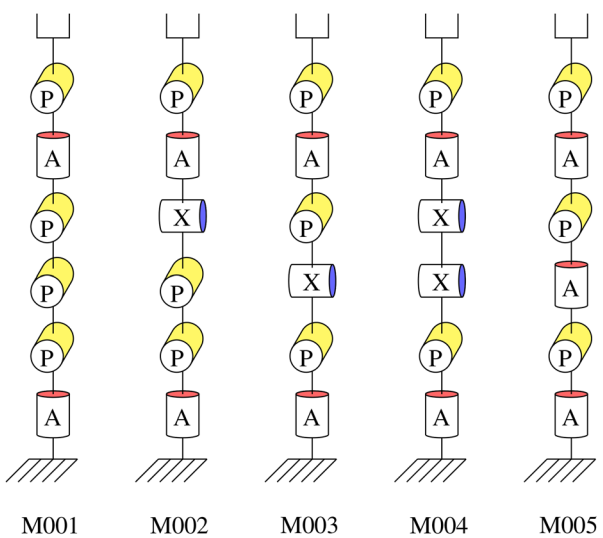

Fig. 5 Candidate kinematic structures

The kinematic structures of the manipulators are designed such that the z-axis of the end-effector frame, Ψ_e, is pointing outward. Besides, the x–y-plane of the test location frame, Ψ_d, is coincident with the tank wall and the z-axis is pointing in the metal. Consequently, both origins should coincide and the z-axes align. The angular error can be determined by taking the inner product of both unit z-axes, $\mathbf{e}_z = (0\ 0\ 1)^{\mathrm{T}}$

$$\cos(\alpha) = \langle \mathbf{R}_d^e \mathbf{e}_z, \mathbf{e}_z \rangle = \mathbf{H}_d^e(3,3) \tag{17}$$

where $\mathbf{R}_d^e$ is the rotation matrix taken from the homogeneous matrix, $\mathbf{H}_d^e$. The left-hand side reduces to the single element $\mathbf{H}_d^e(3,3)$, which is trivial by the definition of a rotation matrix.

The position error, or the distance between the desired pose and the end-effector pose, can be distilled from the relative configuration, $\mathbf{p}_d^e = \mathbf{H}_d^e(1:3,4)$.

To maneuver the end-effector toward the test location, a virtual spring is connected between both. The elastic wrench, induced by this spatial spring, is composed of a rotational and a translational component. The translational component, $\mathbf{F}$, is straightforward

$$\begin{aligned} \mathbf{F} &= k_t \cdot \mathbf{p}_d^e \\ &= k_t \cdot \mathbf{H}_d^e(1:3,4) \end{aligned} \tag{18}$$

with k_t the one-dimensional translational stiffness.

The rotational component of the spatial spring, $\mathbf{m}$, is determined using the cross-product of both z-axes of both the end-effector and the desired pose.

$$\begin{aligned} \mathbf{m}^{\mathrm{T}} &= k_o \cdot \alpha \cdot \frac{\mathbf{e}_z \wedge \mathbf{R}_d^e \mathbf{e}_z}{\sin(\alpha)} \\ &= k_o \cdot \frac{\alpha}{\sin(\alpha)} \begin{pmatrix} -\mathbf{H}_d^e(2,3) \\ \mathbf{H}_d^e(1,3) \\ 0 \end{pmatrix} \end{aligned} \tag{19}$$

where k_o denotes the spring constant of a one-dimensional rotational spring. The total elastic wrench, expressed in end-effector coordinates, becomes $\mathbf{W}^e = (\mathbf{m}\ \mathbf{F})$. Using Eqs. (15) and (16), the updated joint angles are calculated. This is analog to the general spatial compliance described in Sec. 2.3 using

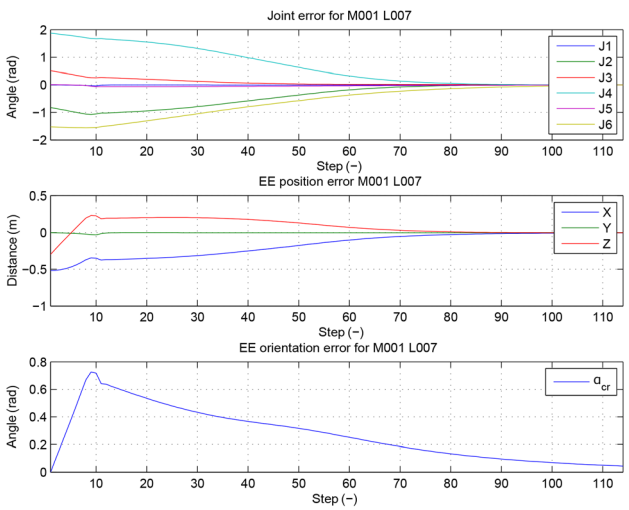

Fig. 6 Joint error, end-effector position error, and end-effector orientation error for manipulator structure M001 at test location L007. This test location is reachable with this manipulator structure: success.

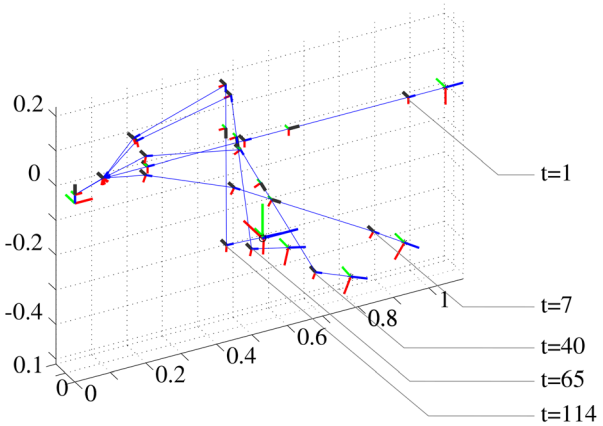

Fig. 7 Overlay in isometric view of kinematic model of manipulator structure M001 at test location L007, during simulation at iterations $t = 1, 7, 40, 65$, and 114

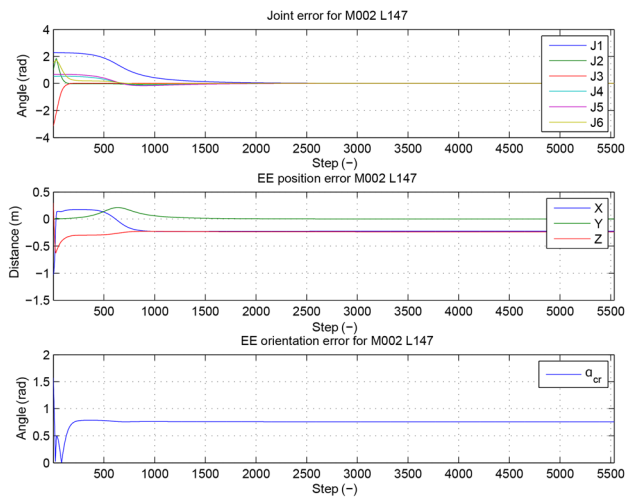

Fig. 8 Joint error, end-effector position error, and end-effector orientation error for manipulator structure M002 at test location L147. This test location is not reachable with this manipulator structure: failure.

$$\mathbf{K} = \begin{pmatrix} \mathbf{K}_t & \mathbf{K}_c \\ \mathbf{K}_c{}^{\mathrm{T}} & \mathbf{K}_o \end{pmatrix} \in \Re^{6\times 6} \tag{20}$$

where

$$\mathbf{K}_t = k_t \begin{pmatrix} 1 & 0 & 0 \\ 0 & 1 & 0 \\ 0 & 0 & 1 \end{pmatrix}, \mathbf{K}_o = k_o \begin{pmatrix} 1 & 0 & 0 \\ 0 & 1 & 0 \\ 0 & 0 & 0 \end{pmatrix}, \mathbf{K}_c = \mathbf{0}$$

For the simulation, the following controller values were empirically determined: $k_t = 1$, $k_o = 0.05$, and $\kappa = 1$. The test location is considered reachable when both $\|\mathbf{p}_d^e\| \leq d_{\mathrm{cr}} = 5\mathrm{mm}$ and $\alpha \leq \alpha_{\mathrm{cr}} = 5\,\mathrm{deg}$.

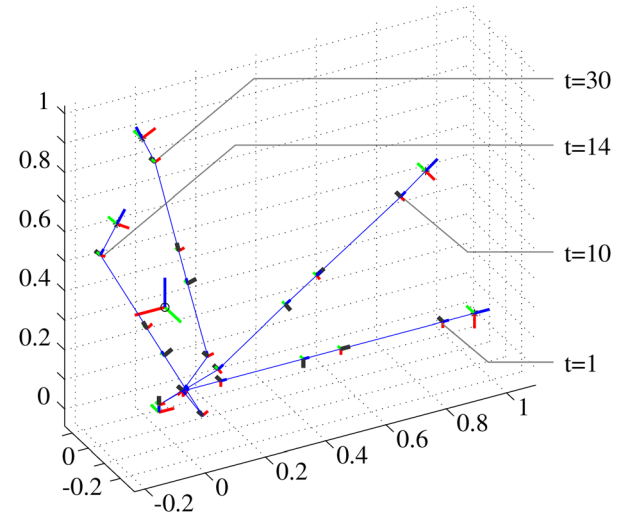

Fig. 9 Overlay in isometric view of kinematic model of manipulator structure M002 at test location L147, during simulation at iterations $t = 1, 10, 14$, and 30

4 Simulation Results

The simulation of the generated candidate structures show that they are all feasible, i.e., all 169 test locations are reachable. However, when gradually reducing the total link down to 1.076 m, structures M001, M002, and M004 showed many failures. Structures M003 and M005 showed successful simulations down to a length of 0.808 m, which is a factor 1.09 larger than the minimum required length of 0.744 m. The only difference between these models is the type of the third joint; in structure M003, this is an X-joint and in structure M005, this is an A-joint.

Figure 6 presents the joint errors, the position and orientation error of the end effector, for manipulator M001 and test location L007. This structure is able to reach the test location within the required error margins and the simulation boundary conditions. Configuration of several iterations of this test run is given in Fig. 7. In contradiction to the successful convergence in Figs. 6 and 7, an unsuccessful trial is given in Figs. 8 and 9; structure M002 at test location L147. In this situation, the simulation is stopped since there was no significant progress; the highest joint velocity is below the threshold.

Table 1 summarizes key results, including the average number of iterations per test location, T_{avg}, and the average conditional number of the manipulator Jacobian, C_{avg}. An upper limit of 10^3 is set for the conditional number; otherwise, the comparison would be hampered by very high values occurring when the manipulator is near a singularity. The conditional number [13] is one way to describe the manipulability of the manipulator at a certain configuration. This figure is the ratio between the largest and the smallest singular value of the geometric Jacobian

Table 1 Summary of the simulation results for the candidate manipulator structures

Manipulator	Length (m)	Failures	Simulation time (s)	Iterations	T_{avg}	C_{avg}	C_{std}
M001 (STg1)	1.076	2	76	68,549	406	37.2	93.8
M002 (STg2)	1.076	53	751	635,998	3763	248.6	371.2
M003 (STg3)	0.826	0	191	159,122	942	31.1	38.4
M004 (STg4)	1.076	18	213	175,221	1037	94.7	563.5
M005 (STg5)	0.826	0	152	126,017	746	16.0	7.2
(STf5)	1.076	0	195	161,797	957	16.0	10.5

Table 2 DH parameters proof-of-principle manipulator structure

Link	a_i (mm)	d_i (mm)	α_i (rad)	θ_i (rad)
1	80	50	$\pi/2$	q_1
2	0	0	$-\pi/2$	q_2
3	0	400	$\pi/2$	q_3
4	0	70	$-\pi/2$	q_4
5	0	465	$\pi/2$	q_5
6	105	0	0	q_6

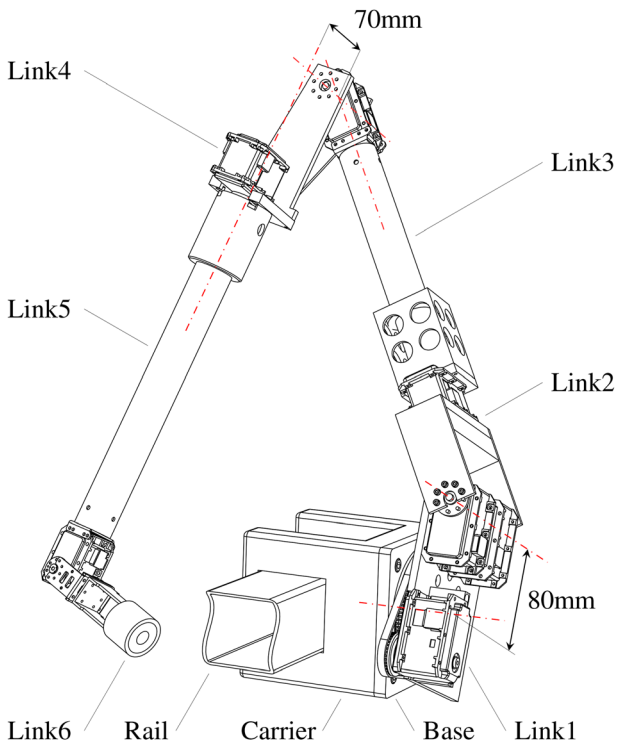

Fig. 10 CAD model based on kinematic structure M005, with indicated joint offsets

Fig. 11 Proof-of-principle manipulator, with covers, mounted on the robot, taking a measurement at one of the test locations

Fig. 12 Robot in experimental ballast water tank, with manipulator folded to a minimum volume

$$C = \frac{\sigma_{\max}(\mathbf{J})}{\sigma_{\min}(\mathbf{J})} \tag{21}$$

When this ratio is large, the Jacobian becomes ill conditioned and the manipulator gets closer to singularity.

From Table 1 can be concluded that manipulators M003 and M005 reach every test locations and that M005 has a significantly lower average condition value. Therefore, this manipulator structure is implemented in a (hardware) proof of principle.

5 Proof of Principle

Based on the simulation results, the kinematic structure M005 is utilized to manufacture a proof of principle for the ballast water tank use case. The DH parameters [23] of this structure are presented in Table 2 and a CAD model is shown in Fig. 10.[1] Dynamixels MX-106 actuate the joints. Customized joints are manufactured, since the Dynamixels are not capable to withstand the bending torque induced on the A-joints. For the first (A-)joint, a THK RA7008C-UU-C0 cross-roller bearing yields the required support stiffness, and has small sizes. A 6 mm GT2 timing belt and corresponding pulleys result in a 36:110 gear ratio for the first joint. The A-joints 3 and 5 consist of coaxial tubes. The outer tube is fixed to the Dynamixel housing, and the inner tube is connected to the output shaft and is supported by a nylon bushing. The joint offset between the first two joints enables the manipulator to maneuver around the rail and the second offset, between joints 4 and 5, makes it possible to fold the arm in a minimum volume. The (intermediate) end effector consists of an electromagnet and forms the basis of the second stage.

The manipulator arm is mounted on a passive carrier pulled by the robot. White plastic covers are added for protecting electronic components and for aesthetic reasons. From a remote system, Dynamixel setpoints are sent via wireless link. This way, a preprogrammed path can be executed or the end effector can be controlled by visual servoing using a 3D mouse.

A photo of the robot, including the manipulator, is given in Fig. 11. The electromagnet is attached to the inner wall of the test tank. Figure 12 shows the manipulator in a folded posture such that it is able to pass through manholes, and in Fig. 13, the manipulator takes measurements under the rail.

6 Evaluation

The method is successfully implemented in a use case scenario, resulting in a manipulator structure that is guaranteed to reach all

[1]Due to time constraints and mixed interest is the proof-of-principle based on a previous version of STg5; the STf5, with a total length of 1076 mm.

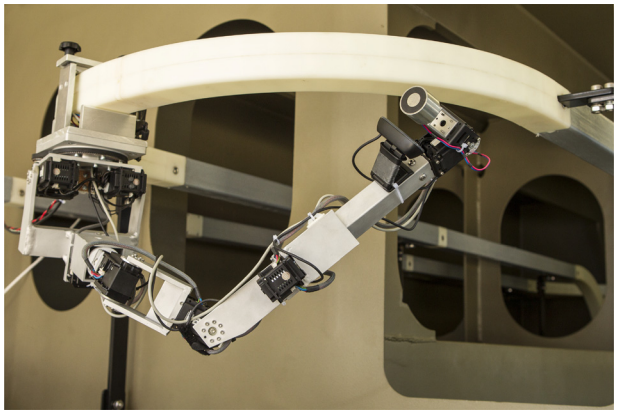

Fig. 13 Proof-of-principle manipulator taking a measurement under the rail

test locations. This is confirmed with a proof of principle in an experimental ballast water tank. The described method is not fully automated since it utilizes the skills and insights of the user. This holds for the design rules and the "scenario simplification" as well. Reducing the possible structures and the set of test location significantly increases the speed of the algorithm and more design iterations can be performed in the same time.

The total stiffness of the elastic wrench can be tuned by κ and the ratio between rotational- and translational-stiffness by k_o, or in the general case, by the stiffness matrices $\boldsymbol{K}_t$, $\boldsymbol{K}_o$, and $\boldsymbol{K}_c$. Values are empirically determined for the given use case and could vary for others.

Joint-space position controllers, like servomotors, can significantly benefit from this algorithm. It solves the inverse kinematics problem and provides the joint angles corresponding to an end-effector pose in cartesian space, given the manipulator structure. Especially, the abovementioned improvements can be used to plan the trajectory in joint space.

Additional feature like collision detection are out of the scope of this paper. However, the practical usability of the design and verification method presented in this paper can significantly improve with collision avoidance.

7 Conclusion

An efficient method to determine the kinematic structure for a manipulator arm is presented. The method starts by reducing the number of combinations to implement joints in the manipulator. Based on defined test locations, the kinematic arm structures are evaluated using key figures like the conditional number and the number of unreachable test locations. The method efficiently determines the kinematic arm structures that are guaranteed to reach all test locations.

The method is successfully applied to a ballast water tank inspection-robot use case. With a set of five design rules, the number of kinematic arm structures was reduced to five. These structures were evaluated at the 169 test locations for reachability using the Jacobian transpose technique, with a spatial geometrical spring.

One configuration had the unique combination of reachability, least link length, and foldability. This configuration has been built using Dynamixel servomotors for a proof of principle. This robot has been extensively tested in a ballast water tank replica at the University of Twente and proved to be able to reach the test locations.

Although the proposed method is applied to a rail-guided use case, it can be applied to mobile robots in general.

Acknowledgment

The authors would like to thank Jop Huttenhuis for his contribution in developing the algorithm and his key role in manufacturing the manipulator arm and his contribution to the RoboShip project and Ronald Aarts for the discussions and his critical feedback on the paper.

This research has been supported by INTERREG IVa; SmartBot—RoboShip.[2]

Nomenclature

$\text{as}(\bullet)$ = antisymmetric part of a matrix; $\text{as}(\mathbf{A}) := (1/2)(\mathbf{A} - \mathbf{A}^{\mathrm{T}})$

$\mathbf{Ad}_{\mathbf{H}_i^j}$ = adjoint transformation; coordinate change of twists

$$\mathbf{T}_{\bullet}^{j,\bullet} = \mathbf{Ad}_{\mathbf{H}_i^j}\mathbf{T}_{\bullet}^{i,\bullet}.\ \mathbf{Ad}_{\mathbf{H}_i^j} := \begin{pmatrix} \mathbf{R}_i^j & \mathbf{0} \\ \tilde{\mathbf{p}}_i^j\mathbf{R}_i^j & \mathbf{R}_i j \end{pmatrix}$$

$\mathbf{H}_i^j$ = homogeneous transformation matrix, $\mathbf{H} \in \mathrm{SE}(3)$; denoting a general coordinate transformation from frame Ψ_i to frame Ψ_j

$\mathbf{J}(\mathbf{q})$ = geometric Jacobian; its columns are the unit-twist expressed in frame Ψ_0. $\mathbf{J}(\mathbf{q}) = \begin{pmatrix} \mathbf{T}_1 & \cdots & \mathbf{T}_n \end{pmatrix}$, such that $\mathbf{T}_n^{0,0} = \mathbf{J}(\mathbf{q})\dot{\mathbf{q}}$

$\mathbf{q}$ = vector of joint variables $\mathbf{q} := \begin{pmatrix} \mathbf{q}_1, \ldots, \mathbf{q}_n \end{pmatrix}^{\mathrm{T}} \in \Re^{n\times 1}$

$\mathbf{R}_i^j$ = rotation matrix, $\mathbf{R} \in SO(3)$; denoting a rotation of frame Ψ_i with respect to frame Ψ_j

$\mathbf{T}_i$ = unit-twist of body i with respect to body $i-1$, expressed in frame Ψ_0; $\mathbf{T}_i := \hat{\mathbf{T}}_i^{0,i-1}$

$\mathbf{T}_i^{k,j}$ = twist, generalized velocity, of body i with respect to body j, expressed in reference-frame k

$\hat{\mathbf{T}}_{\bullet}^{\bullet,\bullet}$ = unit-twist

$\mathbf{W}^i$ = wrench, generalized force; acting on body i, expressed in frame Ψ_i

$\mathbf{W}^{j,i}$ = wrench, generalized force; acting on body i, expressed in frame Ψ_j

Ψ_x = reference frame "x"

$\tilde{\bullet}$ = tilde operator; with the following on-to-one relation between a point and a mapping of points:

$$\mathbf{x} = \begin{pmatrix} x_1 \\ x_2 \\ x_3 \end{pmatrix} \Longleftrightarrow \tilde{\mathbf{x}} = \begin{pmatrix} 0 & -x_3 & x_2 \\ x_3 & 0 & -x_1 \\ -x_2 & x_1 & 0 \end{pmatrix}$$

References

[1] Bischoff, R., Kurth, J., Schreiber, G., Koeppe, R., Albu-Schäffer, A., Beyer, A., Eiberger, O., Haddadin, S., Stemmer, A., Grunwald, G., and Hirzinger, G., 2010, "The KUKA-DLR Lightweight Robot Arm—A New Reference Platform for Robotics Research and Manufacturing," 41st International Symposium on and 26th German Conference on Robotics (ROBOTIK), June 7–9, pp. 1–8.

[2] Universal Robots, 2015, "UR5 Robot: A Highly Flexible Robot Arm," Universal Robots, Odense, Denmark, accessed Dec. 10, 2015, http://www.universal-robots.com/products/ur5-robot

[3] Igus, 2015, "Igus-Robolink: Articulated Joint Modules for Robots," Igus, East Providence, RI, accessed Dec. 10, 2015, http://www.igus.com/wpck/6658/robolink

[4] Festo, 2015, "Bionic Handling Assistant," Festo, Esslingen am Neckar, Germany, accessed Dec. 10, 2015, http://www.festo.com/bionik

[5] Kinova Robotics, 2015, "JACO^2," Kinova Robotics, Boisbriand, Quebec, Canada, accessed Dec. 10, 2015, http://www.kinovarobotics.com/service-robotics

[6] Dwarakanath, T. A., Ghosal, A., and Shrinivase, U., 1994, "Kinematic Analysis and Design of Articulated Manipulators With Joint Motion Constraints," ASME J. Mech. Des., **116**(3), pp. 969–972.

[7] Lee, D., Seo, T., and Kim, J., 2011, "Optimal Design and Workspace Analysis of a Mobile Welding Robot With a 3P3R Serial Manipulator," Rob. Auton. Syst., **59**(10), pp. 813–826.

[8] Baili, M., Wenger, P., and Chablat, D., 2007, "Kinematic Analysis of a Family of 3R Manipulators," IFToMM, Probl. Mech., **15**(2), pp. 27–32.

[9] Bergamaschi, P. R., Saramago, S. F. P., and Nogueira, A. C., 2003, "An Optimal Design of 3R Manipulators Taking Into Account Regular Workspace Boundary," 18th International Congress of Mechanical Engineering, ABCM, Sao Paulo, Brazil, Vol. 1, pp. 86–94.

[10] Lenarčič, J., Stanič, U., and Oblak, P., 1989, "Some Kinematic Considerations for the Design of Robot Manipulators," Rob. Comput.-Integr. Manuf., **5**(2), pp. 235–241.

[11] Wenger, P., 2000, "Some Guidelines for the Kinematic Design of New Manipulators," Mech. Mach. Theory, **35**(3), pp. 437–449.

[2] www.smartbot.eu

[12] Siciliano, B., and Khatib, O., 2007, *Springer Handbook of Robotics*, Springer-Verlag, Secaucus, NJ.
[13] Nakamura, Y., 1990, *Advanced Robotics: Redundancy and Optimization*, 1st ed., Addison-Wesley Longman Publishing, Boston, MA.
[14] Sciavicco, L., and Siciliano, B., 1988, "A Solution Algorithm to the Inverse Kinematic Problem for Redundant Manipulators," IEEE J. Rob. Autom., **4**(4), pp. 403–410.
[15] Stramigioli, S., 2001, *Modeling and IPC Control of Interactive Mechanical Systems: A Coordinate-Free Approach*, Springer-Verlag, New York.
[16] Stramigioli, S., and Bruyninckx, H., 2001, "Geometry and Screw Theory for Robotics," Tutorial (T9), IEEE ICRA 2001, pp. 1–75.
[17] Fasse, E. D., and Broenink, J. F., 1997, "A Spatial Impedance Controller for Robotic Manipulation," IEEE Trans. Rob. Autom., **13**(4), pp. 546–556.
[18] Det Norske Veritas, 2013, "Rules for Classification of Ships—Ships in Operation: Part 7—Survey Requirements," Chap. 1, Hovik, Norway.
[19] Christensen, L., Fischer, N., Kroffke, S., Lemburg, J., and Ahlers, R., 2011, "Cost Effective Autonomous Robots for Ballast Water Tank Inspection," Journal of Ship Production and Design, **27**(3), pp. 127–136.
[20] Christensen, L., Lemburg, J., Vögele, T., Kirchner, F., Fischer, N., Ahlers, R., Psarros, G., and Etzold, L.-E., 2011, "Tank Inspection by Cost Effective Rail Based Robots," 15th International Conference on Computer Applications in Shipbuilding (ICCAS), Trieste, Italy, Sept. 20–22.
[21] Etzold, L.-E., 2011, "Using Robots in Ballast Tanks: Project Under Way to Automate Inspection of Surface Prep and Coating Work," J. Prot. Coat. Linings, (JPCL), (January 2011), pp. 27–36.
[22] Borgerink, D., Stegenga, J., Brouwer, D., Wörtche, H., and Stramigioli, S., 2014, "Rail-Guided Robotic End-Effector Position Error Due to Rail Compliance and Ship Motion," IEEE/RSJ International Conference on Intelligent Robots and Systems, IROS, Chicago, IL, Sept. 14–18, pp. 3463–3468.
[23] Denavit, J., and Hartenberg, R. S., 1955, "A Kinematic Notation for Lower-Pair Mechanisms Based on Matrices," ASME J. Appl. Mech., **22**(2), pp. 215–221.